The Evaluation of Partial Pressures from MD-Simulations of Liquids

A. Klemm

Max-Planck-Institut für Chemie (Otto-Hahn-Institut), Mainz

Z. Naturforsch. **33 a**, 778–781 (1978); received May 3, 1978

Dedicated to Ludwig Waldmann on the occasion of his 65th birthday

In the simulation of liquids by the periodic cube model the pressure can be evaluated by adding up the forces exerted by the particles on one side of a plane on the particles on the other side of the plane, or by an application of the virial theorem. The pressure also occurs in some relations between velocity-velocity- and force-position-autocorrelation functions.

In Molecular Dynamics (MD)-simulations of liquids, pair potentials, a temperature and a density are the usual input data. If the pair potentials are not well chosen or inadequate, the pressure of the MD-system may differ from the pressure of the real liquid to be simulated at the given temperature and density.

Because of the good statistics required it is difficult to evaluate the pressure of an MD-simulation [1]. In most publications of MD-results the pressure is not communicated. If the pressure is communicated [2], it is not clearly said how it was calculated.

It therefore seemed worthwhile, despite the danger of becoming repetitious, to carefully display the relations by which the pressure and the partial pressures of MD-simulated liquids can be evaluated. On this occasion, relations between velocity-velocity- and force-position-autocorrelation functions are also derived.

General

We consider the position-, velocity- and accelerations-vectors $\boldsymbol{r}_i$, $\boldsymbol{v}_i$ and $\boldsymbol{a}_i$, respectively, of a particle i, which is a member of a liquid in thermodynamic equilibrium. No specification is made as to the extent of the liquid. It may be infinite.

For the average of any function $\mathrm{F}(\tau+t)$ over the time τ at constant time t we write

$$\langle \mathrm{F}(\tau+t)\rangle \equiv \lim_{\tau_n\to\infty}\frac{1}{\tau_n}\int_{\tau=0}^{\tau_n}\mathrm{F}(\tau+t)\,\mathrm{d}\tau\,. \tag{1}$$

The interactions between the particles of the liquid cause the velocity of each particle to be isotropic in time:

$$\langle \boldsymbol{v}_i(\tau+t)\rangle = 0\,. \tag{2}$$

From (1) and (2) it follows that

$$\lim_{\tau_n\to\infty}\frac{1}{\tau_n}\boldsymbol{r}_i(\tau_n+t) = 0\,. \tag{3}$$

In accordance with (3)

$$\lim_{\tau_n\to\infty}\frac{1}{\tau_n}\left[\boldsymbol{v}_i(\tau_n)\,\boldsymbol{r}_i(\tau_n+t) - \boldsymbol{v}_i(0)\,\boldsymbol{r}_i(t)\right] = 0\,. \tag{4}$$

The definition (1) enables (4) to be rewritten in the form

$$\left\langle \frac{\mathrm{d}}{\mathrm{d}\tau}\boldsymbol{v}_i(\tau)\,\boldsymbol{r}_i(\tau+t)\right\rangle = 0\,. \tag{5}$$

By performing the differentiation in (5) one gets

$$\langle \boldsymbol{v}_i(\tau)\,\boldsymbol{v}_i(\tau+t)\rangle + \langle \boldsymbol{a}_i(\tau)\,\boldsymbol{r}_i(\tau+t)\rangle = 0\,. \tag{6}$$

The acceleration in (6) can be replaced by the force $\boldsymbol{f}_i$ divided by the particle mass m to yield

$$m\,\langle \boldsymbol{v}_i(\tau)\,\boldsymbol{v}_i(\tau+t)\rangle + \langle \boldsymbol{f}_i(\tau)\,\boldsymbol{r}_i(\tau+t)\rangle = 0\,. \tag{7}$$

Closed System

Before we treat the infinite periodic cube model of MD-simulations we consider the case of a liquid enclosed in a container. The container holds Z particles of the liquid. The force $\boldsymbol{f}_i(\tau)$ can be split into the two terms $\boldsymbol{f}_i^{\mathrm{int}}(\tau)$ and $\boldsymbol{f}_i^{\mathrm{ext}}(\tau)$, where the first term is due to the interactions within the liquid and the second term to the force exerted on the particle i by the solid wall of the container. By doing this and adding up, one obtains from (7)

$$m\,\langle \sum_i^Z \boldsymbol{v}_i(\tau)\,\boldsymbol{v}_i(\tau+t)\rangle + \langle \sum_i^Z \boldsymbol{f}_i^{\mathrm{int}}(\tau)\,\boldsymbol{r}_i(\tau+t)\rangle = -\langle \sum_i^Z \boldsymbol{f}_i^{\mathrm{ext}}(\tau)\,\boldsymbol{r}_i(\tau+t)\rangle\,. \tag{8}$$

If the pressure P is to be calculated from (8), the volume V of the liquid must be known. Since the solid walls of the container consist of atoms which interact with the particles of the liquid by forces which have a certain range, it is impossible to define the volume of the liquid unambiguously. The volume will, however, be the better defined the larger the container is compared with the range of the external forces. We therefore have to consider a container which is large in this sense.

Let the container be idealized by a large cube of volume $V = L^3$ with its edges parallel to and its centre in the origin of our cartesian coordinate system. Due to the large size of the container, the position vector of a particle which feels the external force does not differ by an appreciable percentage from the position vector of the nearest point on the idealized wall of the container itself. One then realizes that in this approximation

$$-\langle \sum_i^Z \mathbf{f}_i^{\mathrm{ext}}(\tau)\,\mathbf{r}_i(\tau+t)\rangle^{\mathrm{b}} = 3PV[1-l(t)/L]. \quad (9)$$

The superscript b indicates that the container is big. $l(t)$ is an effective length. For $t=0, l(t)$ is zero, and for small t-values the magnitude of $l(t)$ is of the order $(Dt)^{1/2}$, where D is the selfdiffusion coefficient of the particles. At infinite time t, $l(t)$ equals L, which corresponds to the fact that a particle which was originally situated near the idealized wall of the container is finally situated with equal probability in any volume element of the container.

From (8) and (9) one gets

$$m\langle \sum_i^Z \mathbf{v}_i(\tau)\,\mathbf{v}_i(\tau+t)\rangle^{\mathrm{b}} + \langle \sum_i^Z \mathbf{f}_i^{\mathrm{int}}(\tau)\,\mathbf{r}_i(\tau+\mathrm{t})\rangle^{\mathrm{b}} = 3PV[1-l(t)/L]. \quad (10)$$

For $t=0$, i.e. $l(t)=0$, (10) reduces to the well known relation usually derived from the virial theorem between the pressure, the kinetic energy, and the internal virial.

It is interesting to note that at times t when the velocity-velocity autocorrelation function, which is independent of L, multiplied with the mass has already decayed to zero, the internal force-position autocorrelation function may still not be zero because on the r.h.s. of (10) the quantity $l(t)/L$, which is dependent on L, is still very small. In this range of large but not too large times t the three-dimensional internal force-position autocorrelation function is practically equal to $3PV$.

Periodic Cube Model

In the periodic cube model of MD-simulations the liquid is infinite in space and is subject to a special initial condition: Each particle belongs to a family of particles which all have the same velocity and are situated on the lattice points of a simple cubic lattice. There are N such families. The lattice constant S and the lattice orientation are the same for all the families, but not so the lattice origin and the velocity. The set of family velocities corresponds to a certain temperature.

Classical mechanics is applied and therefore the spacial periodicity of the initial condition is preserved during the evolution of the liquid. An elementary cube (periodic cube) has an edge length S and holds one particle of each family, i.e. N particles. The particles of a family are called mirror particles. If a particle leaves an elementary cube, a mirror particle of the same family simultaneously enters it.

The definition (1) requires that in calculating $\langle \mathbf{f}_i(\tau)\,\mathbf{r}_i(\tau+t)\rangle$ one has to follow the particle i on its way through the elementary cubes and average over τ. In the case of the periodic cube model, however, we shall use reduced position vectors $\mathbf{r}_i'(\tau+t)$ instead of the position vectors $\mathbf{r}_i(\tau+t)$. The position given by the reduced vector $\mathbf{r}_i'(\tau)$ remains within a given elementary cube by due shifting to mirror particles in the course of the time τ. Because of the unrestricted diffusion of the particles, one has

$$\langle \mathbf{r}_i'(\tau+t)\rangle = \langle \mathbf{r}_i'(\tau)\rangle. \quad (11)$$

$\langle \mathbf{r}_i'(\tau)\rangle$ is the position vector of the centre of a periodic cube. Evidently

$$\langle \mathbf{f}_i(\tau)\,\mathbf{r}_i'(\tau+t)\rangle = \langle \mathbf{f}_i(\tau)\,\mathbf{r}_i(\tau+t)\rangle + S\sum_{s=1}^{\infty}\langle \mathbf{f}_i(\tau)\,\mathbf{n}_i(\tau_s)\rangle, \quad (12)$$

where $\mathbf{n}_i(\tau_s)$ is zero up to a certain time τ_s, when a shift to a mirror particle occurs and therefore $\mathbf{n}_i(\tau_s)$ becomes henceforth a unit vector in the respective direction of one of the cartesian coordinates. $\langle \mathbf{f}_i(\tau+\tau_s)\rangle$ is zero, and therefore the second term on the r.h.s. of (12) is also zero, so that

$$\langle \mathbf{f}_i(\tau)\,\mathbf{r}_i'(\tau+t)\rangle = \langle \mathbf{f}_i(\tau)\,\mathbf{r}_i(\tau+t)\rangle. \quad (13)$$

In order to obtain the pressure P we consider, as in the case of the closed system, a large cube of volume $V=L^3$ holding Z particles, where L is very large compared with the range of the interparticle

forces. The faces of the large cube shall comprise as many faces of the elementary cubes as is necessary to fulfill this requirement.

The internal and external forces acting on the particles in the big cube are exerted by the particles inside and outside this cube, respectively. By introducing these forces and the reduced position vectors, one gets from (7)

$$m\langle \sum_i^Z \boldsymbol{v}_i(\tau)\boldsymbol{v}_i(\tau+t)\rangle + \langle \sum_i^Z \mathbf{f}_i^{\mathrm{int}}(\tau)\boldsymbol{r}_i'(\tau+t)\rangle = -\langle \sum_i^Z \mathbf{f}_i^{\mathrm{ext}}(\tau)\boldsymbol{r}_i'(\tau+t)\rangle. \tag{14}$$

The summations are over the Z particles which are in the big cube at the time τ.

Compared to the case of the closed system, the situation is now different in so far as the particles can diffuse, in the course of the time t, from the "surface" in any direction and not only into the interior of the container. Therefore one now has, instead of (9) and (10),

$$-\langle \sum_i^Z \mathbf{f}_i^{\mathrm{ext}}(\tau)\boldsymbol{r}_i'(\tau+t)\rangle^{\mathrm{b}} = 3PV \tag{15}$$

and

$$m\langle \sum_i^Z \boldsymbol{v}_i(\tau)\boldsymbol{v}_i(\tau+t)\rangle^{\mathrm{b}} + \langle \sum_i^Z \mathbf{f}_i^{\mathrm{int}}(\tau)\boldsymbol{r}_i'(\tau+t)\rangle^{\mathrm{b}} = 3PV. \tag{16}$$

We now discuss the application of (15) and (16) for the calculation of the pressure.

The calculation of the pressure can be achieved by an application of (15) for $t=0$. To do this, we lable the elementary cubes by the three integers α, β and γ, which run from $-\infty$ to ∞ and correspond to the three cartesian coordinates. For the force exerted at the time τ by a particle k in the cube (α, β, γ) on a particle i in the cube $(\alpha', \beta', \gamma')$ we write $\mathbf{f}_{ik}(\alpha', \beta', \gamma', \alpha, \beta, \gamma, \tau)$. By geometrical considerations one then gets from (15) for $t=0$

$$-\sum_{\alpha=1}^{\infty}\sum_{\beta=-\infty}^{\infty}\sum_{\gamma=-\infty}^{\infty}\langle \sum_i^N\sum_k^N \alpha \cdot f_{ik\perp}(0,0,0,\alpha,\beta,\gamma,\tau)\rangle = PS^2, \tag{17}$$

where $f_{ik\perp}$ is the component of $\mathbf{f}_{ik}$ perpendicular to the "surface of the big cube". From (17), two analogous equations are obtained by interchanging in the summations and in the factor before $f_{ik\perp}$ either α with β or α with γ.

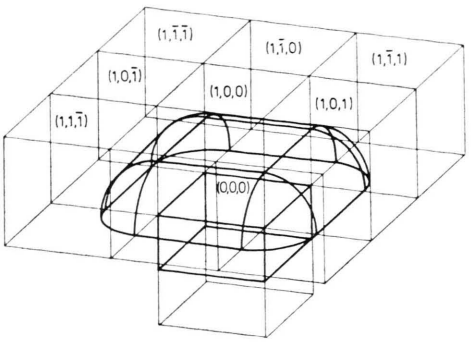

Fig. 1. Within the mushroom-like body shown with heavy lines in the figure there are those particles which are involved in the evaluation of the pressure according to (17), if the cut-off radius of the interparticle forces is half the edge length of the periodic cube. The lables of the periodic cubes are indicated.

In (17) not all the forces $f_{ik\perp}$ contribute significantly to the pressure. In practice, beginning with the 9 cubes for which $\alpha=1$, $\beta=-1, 0, 1$ and $\gamma=-1, 0, 1$, the sums over α, β and γ will successively be increased until the P's thus calculated reach asymptotic values.

Usually, in MD-calculations a cut-off radius for the interparticle forces is introduced. If, for instance, the cut-off radius is chosen to be $S/2$, only the particles inside the mushroom – like body shown in Fig. 1 are involved in the calculation of the pressure according to (17). In order to make full use of the information available, one will calculate the pressure from all six possible "mushrooms" and average.

In the case of ionic liquids the difficulty arises that the Ewald Method in its usual form cannot be applied for the calculation of the external coulombic forces, needed in (17), since this method only yields the total coulombic force acted on a particle.

In the existing literature the pressure has been calculated by an application of (16) for $t=0$, though it is often not clearly said how this was done.

One may be tempted to use (16) for $t=0$ in the form

$$m\langle \sum_i^N \boldsymbol{v}_i(\tau)^2\rangle + \langle \sum_i^N \mathbf{f}_i^{\mathrm{int}}(\tau)\boldsymbol{r}_i'(\tau)\rangle = 3PS^3. \tag{18}$$

If, however, the range of the interparticle forces is of the order of S, the egde length of the periodic cube, the application of (18) can only yield very approximative results for the pressure.

Due to (7) and (13)

$$m\langle \sum_{i}^{N} \boldsymbol{v}_i(\tau)\,\boldsymbol{v}_i(\tau+t)\rangle + \langle \sum_{i}^{N} \mathbf{f}_i(\tau)\,\boldsymbol{r}_i'(\tau+t)\rangle = 0\,. \tag{19}$$

It would certainly be wrong to put the l.h.s. of (19) for $t=0$ equal to $3\,P\,S^3$.

The force $\mathbf{f}_i$ is a sum over j of the pairforces $\mathbf{f}_{ij}$, where $\mathbf{f}_{ij} = -\mathbf{f}_{ji}$. Therefore, (16) can be written in the form

$$m\langle \sum_{i}^{Z} \boldsymbol{v}_i(\tau)\,\boldsymbol{v}_i(\tau+t)\rangle^{\mathrm{b}} + \langle \tfrac{1}{2} \sum_{i}^{Z} \sum_{j}^{Z} \mathbf{f}'_{ij}(\tau) \cdot [\boldsymbol{r}_i'(\tau+t) - \boldsymbol{r}_j'(\tau+t)]\rangle^{\mathrm{b}} = 3\,P\,V\,. \tag{20}$$

The prime at the pairforce indicates that it corresponds to the primed position vectors in the square brackets. The summations in (20) have to be taken over all particles which are in the large cube at a given time τ and zero time t.

The l.h.s. of (20) is proportional to V. The larger V is chosen, the more is it justified to neglect the contribution to the l.h.s. of (20) of those particles which are in the range of the external forces. For the infinite periodic cube model it therefore follows from (20) that

$$m\langle \sum_{i}^{N} \boldsymbol{v}_i(\tau)\,\boldsymbol{v}_i(\tau+t)\rangle + \langle \tfrac{1}{2} \sum_{i}^{N} \sum_{j}^{\infty} \mathbf{f}'_{ij}(\tau) \cdot [\boldsymbol{r}_i'(\tau+t) - \boldsymbol{r}_j'(\tau+t)]\rangle = 3\,P\,S^3. \tag{21}$$

It is practical to calculate the pressure by means of (21) or $t=0$. In doing this, it is often sufficient to restrict the summation over j for a given particle i on those particles j which are within a chosen cutt-off sphere, which possibly reaches into neighbouring cubes, around the particle i, which itself is within the same cube as the other particles i over which the summation in (21) runs.

Partial Pressures

If the liquid consists of z species of particles, so that

$$Z = \sum_{j}^{z} {}^{j}Z, \quad N = \sum_{j}^{z} {}^{j}N, \quad \text{and} \quad P = \sum_{j}^{z} {}^{j}P\,,$$

then in our equations the replacements

$$m \to {}^{j}m\,, \quad \sum_{i}^{Z} \to \sum_{i\in j}^{{}^{j}Z}\,, \quad P \to {}^{j}P\,, \quad l(t) \to {}^{j}l(t)\,,$$

and $$\sum_{i}^{N} \to \sum_{i\in j}^{{}^{j}N}$$

have to be made. One thus gets equations for the calculation of the partial pressures ${}^{j}P$.

Acknowledgement

It is a pleasure to thank Prof. K. Singer, Prof. M. Wolfsberg and Dr. L. Schäfer for discussions which have led to the final version of this paper.

[1] L. Schäfer and A. Klemm, Z. Naturforsch. **31 a**, 1068 (1976). In equation (2) and on page 1070 of this paper, $\boldsymbol{r}_i \sum_{k}^{\infty}$ should be replaced by $\sum_{k}^{\infty}(\boldsymbol{r}_i - \boldsymbol{r}_k)$.

[2] See for example: L. Verlet, Phys. Rev. **159**, 98 (1967); F. H. Stillinger and A. Rahman, J. Chem. Phys. **60**, 1545 (1974), **61**, 4973 (1974); F. Lantelme, P. Turq, B. Quentrec, and J. W. Lewis, Molec. Phys. **28**, 1537 (1974); J. W. Lewis and K. Singer, J. C. S. Faraday II, **71**, 41 (1975).

Fluorescence Detection of Atmospheric SO_2 Using Excitation by NO-γ-Bands

F. Michels, C. Zetzsch, and F. Stuhl *

Ruhr-Universität, Physikalische Chemie I, Bochum

Z. Naturforsch. **33 a**, 782–785 (1978); received April 21, 1978

A method previously applied for the detection of NO was modified to also monitor SO_2. With this method SO_2 is excited by NO-γ-bands ($A^2\Sigma^+ \rightarrow X^2\Pi_r$) and is detected by its subsequent fluorescence in the wavelength region from 300 to 400 nm. The results indicate a linear detection range from 4 ppb to 100 ppm in air using a time response of 100 s. The interferences from some atmospheric constituents were investigated.

Introduction

Recently, it has been shown that NO can be sensitively detected by fluorescence subsequent to excitation by light of the NO-γ-bands [1]. Sulfur dioxide also absorbs light in the wavelength region of the NO-γ-band emission (200 nm $\lesssim \lambda \lesssim$ 250 nm). It has been previously demonstrated that SO_2 fluoresces when excited by Zn (213.8 nm) and Cd (228.8 nm) lines [2] and by light from a deuterium lamp-filter combination (205 nm $< \lambda <$ 225 nm) [3]. Since SO_2 is one of the major air pollutants and since detection methods capable of monitoring more than one atmospheric constituent are desirable, we have studied the feasibility to also detect SO_2 using excitation by NO-γ-bands.

Experimental

In the present study the experimental set up is the same as that used for the detection of NO [1]. Therefore only the major features will be described here. The detector consists of three parts: a lamp to produce NO-γ-bands, a fluorescence cell including a flow system to mix SO_2, and a detection system to monitor the intensity of the fluorescence.

Emission of NO-γ-bands is generated in a microwave discharge in mixtures of flowing air and argon. Light from this lamp is focused into the fluorescence cell through an optical filter (Schott R 220). The reaction cell can be evacuated to less than 1×10^{-5} torr. For the detection of SO_2 the cell was constantly purged with mixtures of pure dry air and SO_2. These mixtures of air and SO_2 were prepared in a flow using a calibrated 5-cm-SO_2-permeation tube (NBS-SRM No 1626). The permeation tube was contained in a thermostat at a constant temperature slightly higher than room temperature. The overall flow was regulated by needle valves and measured by calibrated flowmeters (Rota). Using the full ranges of the available flowmeters, SO_2 mixing ratios ranging from 130 ppb to 10 ppm could be obtained. Only a part of the flowing gas mixture was used to purge the cell. This way the SO_2 mixing ratio could always be kept constant when changing the pressure in the fluorescence cell. In some experiments air was replaced by N_2 or by O_2. In order to add H_2O vapor to SO_2/air mixtures the flow was first fed through a saturator containing liquid H_2O at a temperature of 298 K and then fed through a condensator at lower temperature to control the H_2O pressure. To study interferences from other species known to be present in the atmosphere a number of gases (NO, CH_4, C_2H_6, C_3H_8, C_4H_{10}, C_2H_4, C_3H_6, toluene) were introduced into the flow. These gases were usually injected into a bulb, which was constantly purged by the SO_2/air flow. This way concentrations of about 500 ppm were added initially which subsequently decreased with a time constant of about 30 s. Since NO is known to fluoresce by excitation of the γ-bands [1], NO/air mixtures were prepared in the fluorescence cell as previously [1].

Fluorescence of SO_2 was observed by a photomultiplier through a coloured glass (Schott UG1) which transmits the wavelength interval from about 300 to 400 nm. Photon counting was applied throughout these measurements. For the measurement of SO_2 in ambient air the ratio mode of the photon counter was used. For this purpose a second

---

* On sabbatical leave at NOAA, Aeronomy Laboratory, and CIRES, University of Colorado, Boulder, Colorado 80303.

Reprint requests to Prof. Dr. F. Stuhl, Physikalische Chemie I, Ruhr-Universität, D-4630 Bochum, Germany.

photomultiplier (RCA 1P28) was used to monitor the intensity of the exciting NO-γ-bands. The fluorescence signal was thus registered in reference to the intensity of the incident light. This way, a better long term stability was achieved. Further details of the detection method have been reported elsewhere [1, 4].

Results

Preliminary experiments at low SO_2 concentrations using a static mixing procedure indicated poor reproducibility and non-linear behavior of the fluorescence signal. It is very likely that efficient adsorption processes cause these undesirable effects. All further experiments were therefore performed under flow conditions. This way, a reproducible signal was obtained. However, after a change in $[SO_2]$, it took at least 20 min until a constant signal was reached. To obtain a signal for $[SO_2] = 0$ the fluorescence cell had to be purged with clean air for about 5 hours. In spite of this large time constant for the sampling the electronic time constant was chosen to be 100 s; hence the change of the signal with time could be easily observed.

The influence of different amounts of air on the fluorescence intensity of SO_2 was investigated for a constant pressure of 1×10^{-4} torr SO_2. A Stern-Volmer plot of the result is shown in Figure 1. In this plot the signal is normalized for a pressure of air of 700 torr, since, at this pressure, the fluorescence signal could be determined with higher precision. The half quenching pressure for the SO_2 fluorescence obtained from this figure is 882 torr.

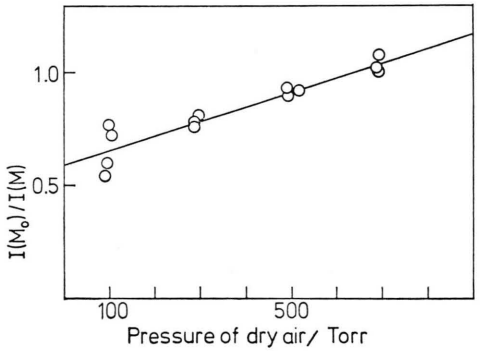

Fig. 1. The inverse of the relative fluorescence intensity $I(M)/I(M)_0$ plotted vs. the pressure of M (M = dry air). The intensity $I(M)_0$ was determined at $[M]_0 = 700$ torr dry air. The SO_2 pressure was constant at 1×10^{-4} torr.

Similar plots obtained for the addition of N_2 and of O_2 resulted in half quenching pressures of 1567 and of 325 torr, respectively. Both these values combined yield a value of 888 torr in very good agreement with the half quenching pressure obtained in Figure 1. These quenching data and those reported in the literature are compared in Table I. The low quenching efficiency of air allows the detector to be operated at relatively high pressures. Therefore all the following experiments were done with air at a pressure of about 720 torr.

Table I. Half quenching pressure, $P_{1/2}$, for the quenching of the SO_2 fluorescence.

Constituent of air	This work [a]	Ref. [3] [b]
N_2	1567	1333
O_2	325	373
air (calculated)	888	877
air (measured)	882	862
H_2O	(19) [c]	16.5) [c]

[a] $[SO_2] = 1$ to 3×10^{-4} torr. [b] $[SO_2] = 10^{-1}$ torr.
[c] Non-linear Stern-Volmer plot.

Water is present in ambient air at variable concentrations. Stern-Volmer plots for the addition of water to SO_2/air mixtures were found to be non-linear. Figure 2 displays the relative intensity of the fluorescence signal as a function of the pressure of H_2O. In this figure the signal is normalized for the absence of H_2O. H_2O was added to 200 ppb (circles) and to 365 ppb (squares) SO_2 in air at 720 torr. Included in this figure are two bars representing the range of previous data obtained by

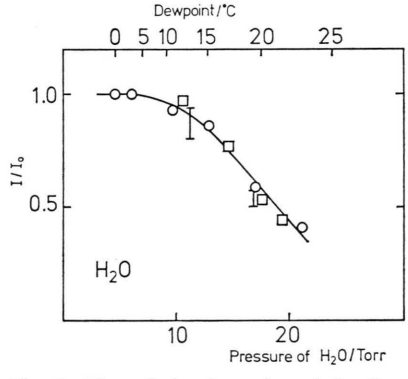

Fig. 2. The relative intensity of the fluorescence as a function of added H_2O. The intensity in the absence of H_2O was taken as a reference. Experimental conditions: ○ 200 ppb SO_2 in 720 torr air; □ 365 ppb SO_2 in 720 torr air. The range of data previously measured [2] is indicated by bars.

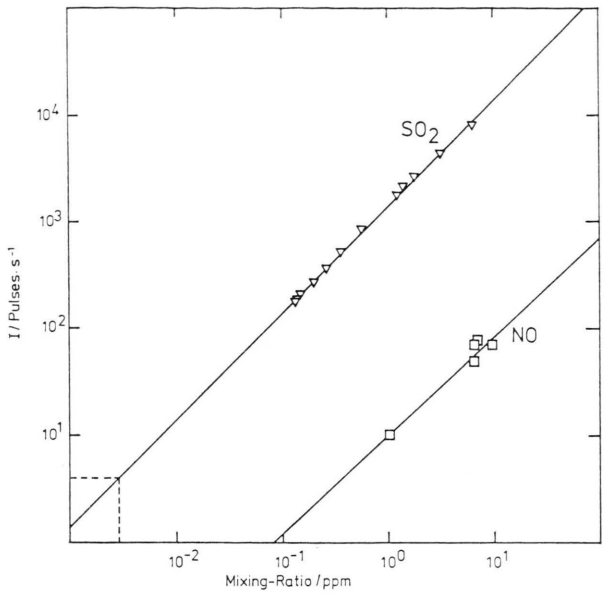

Fig. 3. Calibration curve of the SO_2 detector in a double logarithmic plot. The fluorescence intensity is given in number of photon pulses per sec. and the concentration is given by the mixing ratio. The overall pressure was 720 torr and the time constant was 100 s. The detection limit (three standard deviations of the background signal) is indicated by the dashed line. The average background signal is subtracted. The fluorescence signal for the addition of NO is included.

Schwartz et al. [2] using a Cd lamp. The data of Fig. 2 show that the fluorescence signal is reduced by a factor of 2 at 100% and by a factor of 1.03 at 50% relative humidity at 20 °C air temperature.

Figure 3 displays the dependence of the fluorescence intensity on the mixing ratio of SO_2 in dry air. It is evident from this figure that the intensity of the fluorescence is linearly dependent on the concentration of SO_2 in the range from 130 ppb to 7 ppm. A number of similar linear plots were obtained for slightly different experimental arrangements (using different light collection efficiencies of the detection system). Also, a linear relationship was obtained using the ratio mode of the photon counter. At the low concentrations of Fig. 3 a linear dependence of the fluorescence intensity on the concentration is expected since self-quenching by added SO_2 is a negligible process. Furthermore, it can be shown that the amount of light absorbed by SO_2 is linearly dependent on $[SO_2]$ at these low concentrations. Because of these reasons we have represented the calibration curve of Fig. 3 by a straight line with the slope one. In this figure the average background signal has been subtracted. This background signal was about 120 pulses s^{-1} and was caused by both the dark current of the photomultiplier and by a weak unknown fluorescence. The linear extrapolation of the calibration curve in Fig. 3 is equal to three times the standard deviation (3σ) of the background signal at a mixing ratio of 4 ppb SO_2 (dashed line). This value provides a measure for the detection limit of the present apparatus when using a time constant of 100 s.

Recently it has been shown that NO fluoresces efficiently at about 250 nm when excited by NO-γ-bands [1]. We have therefore investigated the interference of fluorescing NO on the detection of SO_2. Figure 3 shows the fluorescence signal for the addition of NO obtained in the wavelength region from 300 to 400 nm. From these data it can be seen that NO fluoresces about 100 times weaker than SO_2 at the same mixing ratio. A similar result was obtained previously by Okabe et al. [5]. Moreover, Okabe et al. have added a number of gases to their system using irradition by Zn and Cd lamps and have found no significant interference by the gases studied [5]. In the present investigation we have added CH_4, C_2H_6, C_3H_8, C_4H_{10}, C_2H_4, C_3H_6 and have observed no interfering fluorescence. C_7H_8 (toluene) was found to interfere less than NO did.

All other tropospheric constituents are present at relatively low mixing ratios. Those with mixing ratios greater than 1 ppm are usually present at constant mixing ratios. Furthermore they do not absorb light of the incident NO-γ-band irradiation. Therefore these trace gases are considered not to interfere with the detection of SO_2 in tropospheric

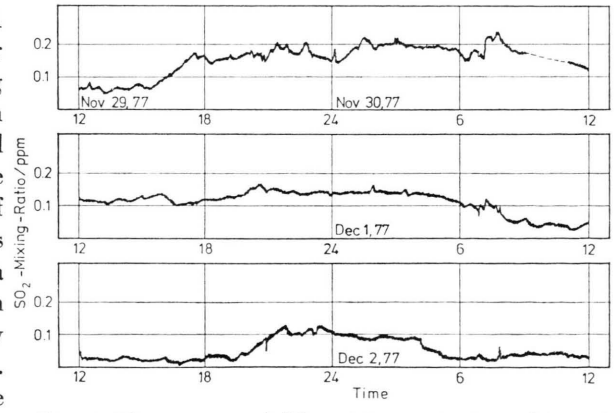

Fig. 4. Measurement of SO_2 mixing ratios in ambient air during the period of Nov. 29, 1977, to Dec. 2, 1977. Sampling site was Building NC at the Ruhr University Bochum. Time constant used: 100 s; air temperature: ≈ 5 °C.

air. Minor trace gases (<1 ppm) are not likely to be able to quench the fluorescence or to decrease the incident light intensity by absorption because of their low concentrations.

To demonstrate the feasibility of the present method we have monitored ambient air at the Ruhr-University Bochum. The measured mixing ratios of SO_2 during three consecutive days (Nov. 29 until Dec. 2, 1977) are shown in Figure 4. It should be noted that during these days the outside temperature was always less than 5 °C and hence the humidity (Fig. 2) is not expected to influence the data very much. Figure 4 shows that mixing ratios of up to 0.25 ppm SO_2 (corresponding to ≈ 0.7 mg m^{-3}) were observed.

Discussion

The present detection method permits NO and SO_2 to be monitored simultaneously in polluted air. In air irradiated by NO-γ-bands fluorescence of NO is monitored at (250 ± 10) nm and fluorescence of SO_2 is monitored in the wavelength region from 300 to 400 nm. Thus either two photomultiplier/filter combinations or one photomultiplier with two alternating filters can be used to measure NO and SO_2 at the same time. Since the most favorable pressures for the detection of NO (35 torr) and of SO_2 (>720 torr) are different, a pressure of about 300 torr in the fluorescence cell should be chosen as a compromise for the simultaneous detection. This way the detection limit (3σ) will stay below about 10 ppb for both gases. Also the interference in the detection of SO_2 by H_2O will become much smaller. A linear response for both constituents has been shown for up to 10 ppm. The long time constant we observe for the signal is very likely to be due to surface processes in the sampling lines and in the fluorescence cell. Different materials and a heated system can possibly decrease the time constant.

Recently Okabe and coworkers [2, 6] have developed a fluorescence method capable of monitoring both NO and SO_2 using irradiation by the Zn 213.8 nm line. The fluorescence was detected in the wavelength region from about 230 to 420 nm. The reported detection limits of this method are: 10 ppb (signal to noise ratio = 1) NO in N_2; 0.5 ppm NO in air; and 8.6 ppb (standard deviation 29%) SO_2 in air. Since SO_2 can interfere when NO is monitored, the use of different wavelength regions for the detection of SO_2 and of NO fluorescence has been considered [6]. This method has been used for the measurement of NO in standard reference mixtures of NO in N_2 and for the measurement of SO_2 in air, stack gases and automobile exhaust.

Okabe and coworkers have also studied the feasibility of exciting SO_2 by the Cd 228.8 nm line [2] and by a 216 nm deuterium source [3]. However, from the published work, none of these methods seems to be more favorable for air monitoring than the exication by the Zn line. Previously Zolner et al. [7] have excited SO_2 by a flash lamp and have monitored SO_2 by its fluorescence. The detection limit of this method has been reported to be 0.5 ppm.

The excitation and fluorescence processes of SO_2 have been described by Okabe and coworkers in detail [2, 3, 5, 6] and will not be discussed here. These authors have studied the influence of a number of gases on the fluorescence signal. In the present study we have repeated some of their experiments at about 10^3 times lower concentrations of SO_2 and find reasonable agreement with their results.

The mixing ratios observed in ambient air (Fig. 4) were compared with those obtained by the Landesanstalt für Immisionsschutz NRW" [8] at the air monitoring station Bochum-Stadtmitte. Considering the distance of 6 km between the two sampling sites the agreement was found to be satisfactory. A maximum value of 0.7 mg m^{-3}, for example, was measured at both sites at the same time.

Acknowledgement

We thank the "Ministerium für Wissenschaft und Forschung des Landes Nordrhein-Westfalen" for financial support.

[1] K. Höinghaus, H. W. Biermann, C. Zetsch, and F. Stuhl, Z. Naturforsch. **31 a**, 239 (1976).
[2] F. P. Schwarz, H. Okabe, and J. K. Wittaker, Anal. Chem. **46**, 1024 (1974).
[3] H. Okabe, Anal. Chem. **48**, 1487 (1976).
[4] F. Michels, Diplomarbeit, Ruhr-Universität Bochum (1977).
[5] H. Okabe, P. L. Splitstone, and J. J. Ball, J. Air. Poll. Contr. Ass. **23**, 514 (1973).
[6] F. P. Schwarz and H. Okabe, Anal. Chem. **47**, 703 (1975).
[7] W. J. Zolner, D. J. Mayer, and D. A. Helm, Anal. Instrum. **12**, 9 (1974).
[8] We thank Dr. Bach, Landesanstalt für Immissionsschutz NRW, for providing us with the data.

On the Green-To-Red Line Intensity Ratio in the Solar Corona

H. P. Mital and U. Narain

Astrophysics Research Group, Physics Department, Meerut College, Meerut, India

Z. Naturforsch. **33a**, 786–788 (1978); received January 5, 1978

Green-to-red line intensity ratios have been investigated by including various processes, like radiative recombination via bound levels, autoionization, dielectronic recombination, etc. An improvement in the value of coronal temperature is found.

1. Introduction

The determination of the intensity ratio of the green line of FeXIV (λ 5303 Å) to the red line of FeX (λ 6374 Å) has become an important method of establishing the temperature distribution in the solar corona (Schwartz and Zirin [1], Kang and Arny [2], Allen and Dupree [3], and Narain and Chandra [4, 5]).

In the present investigation we present improved line intensity ratios by taking various processes into consideration.

The green-to-red line intensity ratio may be evaluated by the expression (Chandra and Narain [6]):

$$\frac{I_{5303}}{I_{6374}} = 1.74 \cdot \frac{(\mathrm{Ni})_{\mathrm{XIV}}}{(\mathrm{Ni})_{\mathrm{X}}} \cdot \exp\{-4.64 \times 10^3/T\},$$

which differs from those given by Schwartz and Zirin [1] and Billings [7] by a constant factor.

For the evaluation of $(\mathrm{Ni})_{\mathrm{XIV}}/(\mathrm{Ni})_{\mathrm{X}}$ (the ratio of relative abundances of FeXIV and FeX ions) Narain and Chandra [4] used the dielectronic recombination rate coefficients which were obtained by multiplying the radiative ones by 20 times the number of the outer shell electrons of the recombining ion, following Burgess and Seaton [8]. This probably leads to overestimation. Further, they did not include the other important processes such as radiative recombination via bound levels and autoionization. Although Jordan [9] included these processes in her computations, she did not use the general formula given by Lotz [10] for collisional ionization rates which includes Seaton's [11] formula as a special case in the low energy region (Chandra and Narain [12]).

Burgess and Summers [13] and Summers [14] investigated the effect of electron and radiation density on the process of dielectronic recombination and ionization balance. They came to the conclusion that electron density effects are negligible below a certain critical value for heavier coronal ions. Blaha [15] investigated the effect of secondary autoionization and concluded that the process is important for Fe^{+9} to Fe^{+13}. Summers [16] investigated the ionization equilibrium of various elements over most of their ionization stages. He included secondary autoionization in his study. Very recently Jacobs et al. [17] investigated the influence of autoionization accompanied by excitation on the process of dielectronic recombination. Some reduction in the values of the coefficients was observed.

In face of these new facts it becomes desirable to reinvestigate the green-to-red line intensity ratio and thereby the temperature distribution in the solar corona.

Reprint requests to Dr. H. P. Mital, Astrophysics Research Group, Physics Department, Meerut College, Meerut, Indien.

2. Theoretical Details

Here we have computed the ratio of relative abundances by taking various processes into consideration:

(i) Direct collisional ionization from the ground state; $q_c(X^{+m})$: Following Lotz [10] the ionization rate coefficients are given by:

$$q_c = 3.8 \times 10^{-9}\ \mathrm{cm^3\ sec^{-1}} \sum_i q_i \times \left(\frac{10^6\ \mathrm{K}}{T}\right)^{3/2} \left(\frac{P_i}{kT}\right)^{-1} \int_{P_i/kT}^{\infty} \frac{e^{-x}}{x}\,\mathrm{d}x$$

where q_i is the number of equivalent electrons, P_i the binding energy of the ith subshell of the target, and the other symbols have their usual meaning.

(ii) Collisional excitation followed by autoionization: $q_{\mathrm{auto}}(X^{+m})$, which has been computed by the approach of Seaton [11] and Jordan [9].

(iii) Radiative recombination via continuum $\alpha_c(X^{+m})$. For this the expressions of Elwert [18] and Burgess and Seaton [8] have been used.

(iv) Radiative recombination via bound levels $\alpha_b(X^{+m})$ has been computed by the expression of Wilson [19].

(v) Dielectronic recombination: The dielectronic recombination rate coefficients have been computed by the Burgess [20] general formula

$$\alpha_d = \frac{8.2\times10^{-4}}{T^{3/2}} \times \frac{Z^{1/2}(Z+1)^2}{(Z^2+13.4)^{1/2}} \times \sum_j \frac{F(j\to i)\, E_0{}^{1/2}}{(1+0.105x+0.015x^2)} \exp\{-E_0/kT\}$$

where $x = 0.0735 E_0 (Z+1)^{-1}$, E_0 is in eV, T in K, E_0 is the energy and f the oscillator strength for the resonance transition $i \to j$ in the recombining ion. Z is the charge on the recombining ion. The expression is summed over the strong resonance levels j to obtain a total recombination rate (Gabriel and Jordan [21]).

Thus

$$\frac{N(X^{+m+1})}{N(X^{+m})} = \frac{q_c + q_{auto}}{\alpha_c + \alpha_b + \alpha_d} = \frac{q_{tot}(X^{+m})}{\alpha_{tot}(X^{+m})}$$

and

$$\frac{N(Fe^{+13})}{N(Fe^{+9})} = \prod_{m=9}^{12} \frac{q_{tot}(X^{+m})}{\alpha_{tot}(X^{+m})} .$$

3. Results and Discussion

The intensity ratios so computed are displayed in Fig. 1 as a function of temperature along with those using Table 10 of Jordan [9] and Narain and Chandra [4]. For the sake of clarity others have been lett from comparison.

It is obvious from the figure that the temperature at which the two lines are of equal intensity is 1.8 MK. This is in closest agreement with the line width results assuming thermal broadening (Billings [22]) of all the previous ones. The corresponding result, using Jordans' [9] data, is 1.4 MK. Since Lotz's [10] ionization cross sections are somewhat larger than Seaton's [11] they can't be responsible for our curve lying below Jordan's curve. The discrepancy reflects the larger recombination coefficient (mainly dielectronic) used by us. Apparently Jordan [9] overestimates the effect of pressure diminishing the dielectronic recombination rate. A similar observation has also been made by Jacobs et al. [17].

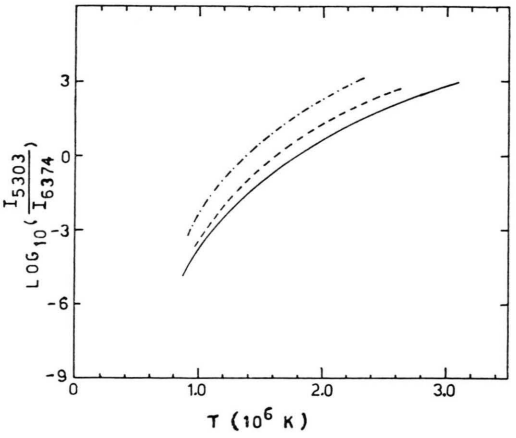

Fig. 1. Green-to-red line intensity ratio versus temperature in the solar corona. ——— Present; ----- Narain and Chandra (1975); -·-·- Calculation using Table 10 of Jordan (1969).

It may also be remarked that the effect of autoionization accompanied by excitation on intensity ratios is much smaller and the effect of photoionization is negligible.

Acknowledgements

We are grateful to Professor S. P. Khare and Professor S. K. Joshi and Dr. S. M. R. Ansari for their encouragements. Financial assistance provided by UGC, New Delhi is also thankfully acknowledged. The computation was done on an IBM 360/44 at Delhi University Computer Centre.

[1] S. B. Schwartz and H. Zirin, Astrophys. J. **130**, 384 (1959).
[2] I. J. Kang and T. A. Amy, Astrophys. J. **153**, 325 (1968).
[3] J. W. Allen and A. K. Dupree, Astrophys. J. **155**, 27 (1969).
[4] U. Narain and S. Chandra, Astrophys. J. **200**, 234 (1975).
[5] U. Narain and S. Chandra, Solar Phys. **47**, 607 (1976).
[6] S. Chandra and U. Narain, Solar Phys. **46**, 183 (1976).
[7] D. E. Billings, A guide to the solar Corona, Academic Press, London 1966, p. 240.
[8] A. Burgess and M. J. Seaton, Mon. Not. Roy. Astron. Soc. **127**, 355 (1964).
[9] C. Jordan, Mon. Not. Roy. Astron. Soc. **142**, 501 (1969).
[10] W. Lotz, Z. Phys. **216**, 241 (1968).
[11] M. J. Seaton, Planet. Space Sci. **12**, 55 (1964).

[12] S. Chandra and U. Narain, Indian J. Pure. Appl. Phys. **13**, 276 (1975).
[13] A. Burgess and H. P. Summers, Astrophys. J. **157**, 1007 (1969).
[14] H. P. Summers, Mon. Not. Roy. Astron. Soc. **158**, 255 (1972).
[15] M. Blaha, Astrophys. Letters **10**, 179 (1972).
[16] H. P. Summers, Mon. Not. Roy. Astron. Soc. **169**, 663 (1974).
[17] V. L. Jacobs, J. Davis, P. C. Kepple, and M. Blaha, Astrophys. J. **211**, 605 (1977).
[18] G. Elwert, Z. Naturforsch. **7a**, 703 (1952).
[19] R. Wilson, Plasma in Space and in Laboratory ESRO SP (1967), p. 373.
[20] A. Burgess, Astrophys. J. **141**, 1588 (1965).
[21] A. H. Gabriel and C. Jordan, in Case Studies in Atomic Collision Physics, ed. E. W. McDaniel and M. R. C. McDowell Vol. **2**, 1972, p. 220.
[22] D. E. Billings, Symp. on Solar Spectrum, Utrecht 1963.

Ballooning Modes in Three-dimensional MHD Equilibria with Shear

D. Correa-Restrepo

Max-Planck-Institut für Plasmaphysik, Garching bei München, Federal Republic of Germany

Z. Naturforsch. **33a**, 789–791 (1978); received April 22, 1978

Stability with respect to ballooning modes in arbitrary, three-dimensional, ideal MHD equilibria with shear is studied. The destabilizing perturbations considered here have finite gradients along the field and are localized around a closed magnetic field line, the localization being weaker on the surface than transversally to it. This kind of localization allows the problem of stability to be reduced to the solution of a one-dimensional eigenvalue problem.

The possibility of deriving a stability criterion for perturbations localized around a closed magnetic field line has been suggested by Mercier et al. [1, 2]. However, no conclusive results have yet been presented, owing mainly to the difficulties arising from the presence of shear. By properly choosing the localized perturbations, it is shown here that the problem of stability can be reduced to the solution of a one-dimensional eigenvalue problem. This result, valid for general three-dimensional equilibria, is equivalent in the case of axial symmetry to the results obtained by Connor et al. [3] for ballooning instabilities with high toroidal mode number, which have also been investigated recently by Dobrott et al. [4] and, in the case of a large-aspect-ratio axisymmetric toroidal configuration by Coppi [5]. According to the energy principle, we can express the change δW in potential energy due to a displacement which vanishes at the plasma surface as

$$\delta W = \frac{1}{2}\int \mathrm{d}\tau \Big[B^{-2}\,|\boldsymbol{Q}\times\boldsymbol{B}|^2 + B^{-2}\,|\boldsymbol{Q}\cdot\boldsymbol{B} - \boldsymbol{\xi}\cdot\nabla p|^2 + \gamma p\,|\nabla\cdot\boldsymbol{\xi}|^2 + \frac{\boldsymbol{B}\cdot\boldsymbol{j}\,B^{-2}}{2}\{(\boldsymbol{B}\times\boldsymbol{\xi}^*)\cdot\boldsymbol{Q} + (\boldsymbol{B}\times\boldsymbol{\xi})\cdot\boldsymbol{Q}^*\} - \{(\boldsymbol{\xi}\cdot\nabla p)(\boldsymbol{\xi}^*\cdot\boldsymbol{\varkappa}) + (\boldsymbol{\xi}^*\cdot\nabla p)(\boldsymbol{\xi}\cdot\boldsymbol{\varkappa})\}\Big], \quad \boldsymbol{\varkappa} = \left(\frac{\boldsymbol{B}}{B}\cdot\nabla\right)\frac{\boldsymbol{B}}{B}, \tag{1}$$

all the symbols having their usual meaning.

To describe our system, we employ coordinates v, θ, $\varphi = \zeta - q_0\theta$, where v, θ, ζ are Hamada coordinates [7] and $q_0 = M/N$ (M, N integers) is the safety factor of the rational surface on which the localization line lies. In this coordinate system, the physical quantities are periodic in θ, with period N, and in φ, with period 1:

$$\begin{aligned}\Phi(\theta,\varphi) &= \Phi(\theta,\varphi+1)\\ &= \Phi(\theta+1,\varphi-M/N)\\ &= \Phi(\theta+N,\varphi).\end{aligned}$$

The magnetic field $\boldsymbol{B}$ and the gradient along a field line can be expressed as

$$\begin{aligned}\boldsymbol{B} &= \dot{\chi}[\nabla\varphi\times\nabla v + (q-q_0)\nabla v\times\nabla\theta],\\ \boldsymbol{B}\cdot\nabla &= \dot{\chi}[\partial_\theta + (q-q_0)\partial_\varphi],\end{aligned}$$

with $q = \dot{\Psi}/\dot{\chi}$. Ψ and χ are the longitudinal and transversal magnetic fluxes respectively. Dots mean derivatives with respect to the volume. Thus

$$q_0 = \dot{\Psi}/\dot{\chi}(v = v_0).$$

Setting

$$\boldsymbol{\xi} = U\nabla\theta\times\nabla\varphi + T\nabla v\times\nabla\theta + S\boldsymbol{B},$$

we obtain

$$\begin{aligned}\boldsymbol{Q}\times\boldsymbol{B} &= -\dot{\chi}[(\boldsymbol{B}\cdot\nabla T - \dot{q}\dot{\chi}U)\nabla v + (q-q_0)(\boldsymbol{B}\cdot\nabla U)\nabla\theta - (\boldsymbol{B}\cdot\nabla U)\nabla\varphi],\\ \boldsymbol{Q}\cdot\boldsymbol{B} - \boldsymbol{\xi}\cdot\nabla p &= -B^2[2(U\varkappa_v + T\varkappa_\varphi) + \partial_v U + \partial_\varphi T - \boldsymbol{B}\cdot\nabla\{B^{-2}(UB_v + TB_\varphi)\}],\\ \nabla\cdot\boldsymbol{\xi} &= \partial_v U + \partial_\varphi T + \boldsymbol{B}\cdot\nabla S,\\ \boldsymbol{B}\times\boldsymbol{\xi}^*\cdot\boldsymbol{Q} &= \dot{\chi}[T^*(\boldsymbol{B}\cdot\nabla U) - U^*(\boldsymbol{B}\cdot\nabla T) + \dot{q}\dot{\chi}\,|U|^2],\\ (\boldsymbol{\xi}\cdot\nabla p)(\boldsymbol{\xi}^*\cdot\boldsymbol{\varkappa}) &= p[\varkappa_v|U|^2 + \varkappa_\varphi UT^*],\end{aligned}$$

Reprint requests to D. Correa-Restrepo, Max-Planck-Institut für Plasmaphysik, D-8046 Garching bei München.

where B_v, B_φ, $\varkappa_v$ and $\varkappa_\varphi$ are covariant components of $\boldsymbol{B}$ and $\boldsymbol{\varkappa}$ respectively. We now specify the type of test functions we consider here: The perturbations are localized around a closed field line, defined by $v=v_0$, $\varphi=\varphi_0$, and have $\boldsymbol{B}\cdot\nabla/\dot{\chi}\sim 0(1)$, i.e. finite derivatives along the field. Setting

$$t=\frac{v-v_0}{v_0\varepsilon^3}\,,\quad x=\frac{\varphi-\varphi_0}{\varepsilon^3}$$

with $\varepsilon\ll 1$, we require that $\partial_t\sim\partial_x\sim 0(1)$, when applied to perturbations. Thus, derivatives transversal to the field are large, of order ε^{-3}. Furthermore the perturbations are required to vanish for $|v-v_0|\geqq v_0\varepsilon^2$ (i.e. $|t|\geqq\varepsilon^{-1}$), $|\varphi-\varphi_0|\geqq\varepsilon$ (i.e. $|x|\geqq\varepsilon^{-2}$) and are therefore more strongly localized across the surfaces than on them. (It will be seen that the test functions we give later are consistent with these assumptions.)

We now expand the equilibrium quantities $A(v,\theta,\varphi)$ in a Taylor series around $v=v_0$, $\varphi=\varphi_0$:

$$A(v,\theta,\varphi)=A(v_0,\theta,\varphi_0)+\frac{\partial A}{\partial\varphi}(v_0,\theta,\varphi_0)(\varphi-\varphi_0)+0(\varepsilon^2)\,,$$

and the test functions U, T, S in a series of the form

$$U=U_0+U_1\varepsilon+U_2\varepsilon^2+U_3\varepsilon^3+\cdots,$$

where the order of magnitude of the different terms is given by the powers of ε and the functions U_i may depend implicitly on ε (similarly for T and S) and obtain from the lowest order δW the following conditions: $U_1=U_2=T_1=T_2=0$. (We could set $\partial_t U_1+v_0\partial_x T_1=\partial_t U_2+v_0\partial_x T_2=0$ but this has no effect on the lowest order δW.) $\partial_t U_0+v_0\partial_x T_0=0$, i.e. $U_0=v_0\Phi_x$, $T_0=-\Phi_t$ (otherwise, δW will be positive).

Then, in this approximation, the term in the potential energy due to the interaction of the magnetic field with the current is an exact differential which vanishes after integration.

For quilibria with shear, the fluid compression term $\gamma\nabla\cdot\boldsymbol{\xi}$ can be made to vanish by exploiting the freedom in S_0 if we require that $\iint \mathrm{d}x\mathrm{d}\theta\, U_3=0$ [8].

Finally, the field line compression term

$$\boldsymbol{Q}\cdot\boldsymbol{B}-\boldsymbol{\xi}\cdot\nabla p$$

can be eliminated with the help of the functions U_3 and T_3, provided that Φ_x and Φ_t have a vanishing mean value $\iint\Phi_x\mathrm{d}x\mathrm{d}\theta=\iint\Phi_t\mathrm{d}x\mathrm{d}\theta=0$. Thus, in an expansion in ε, the leading order contribution to δW is

$$\delta W_0=\frac{v_0\varepsilon^6}{2}\int_{-\varepsilon^{-1}}^{\varepsilon^{-1}}\mathrm{d}t\int_{-\varepsilon^{-2}}^{\varepsilon^{-2}}\mathrm{d}x\int_0^N\mathrm{d}\theta\left[B^{-2}\dot{\chi}^4\left|\nabla v\frac{\partial}{\partial t}\frac{\boldsymbol{B}\cdot\nabla\Phi}{\dot{\chi}}+v_0\nabla\varphi\frac{\boldsymbol{B}\cdot\nabla\Phi_x}{\dot{\chi}}\right|^2-2\dot{p}\left\{v_0^2\varkappa_v|\Phi_x|^2-\frac{v_0}{2}\varkappa_\varphi(\Phi_x\Phi_t^*+\Phi_x^*\Phi_t)\right\}\right],\tag{2}$$

where the equilibrium quantities depend only on θ, the variable along the localization line (v_0 and φ_0 enter the calculations only as parameters).

The stabilizing term in δW_0 represents the work done against the tension of the magnetic field lines. The non-positive-definite term arises from the interaction of the perturbation with the magnetic line curvature. We now consider a particular class of localized test functions:

$$\Phi(t,x,\theta)=f(\varepsilon t,\varepsilon^2 x)\exp\{i\alpha(x-\dot{q}\,v_0 t\,\theta)\}\cdot\sum_n\exp\{i\alpha\dot{q}\,v_0\,n\,N\,t\}\,F(\theta-nN),\quad f\sim 0(1),\tag{3}$$

where f, f_x, f_t vary slowly with both t and x and are localized, i.e. vanish for $|t|\geqq\varepsilon^{-1}$, $|x|\geqq\varepsilon^{-2}$. $\alpha\sim 0(1)$ is an arbitrary constant and $F\in L_2$ in $-\infty<\theta<\infty$ (we may consider functions $F(\theta)\in L_2$, since these can always be approximated by a sequence of functions $F_n(\theta)$, each of which is continuous and of bounded variation over a finite interval). Then, $\Phi\in L_2$ in $0\leqq\theta\leqq N$. Φ is obviously periodic in θ, with period N. Furthermore, to lowest order

$$\frac{\boldsymbol{B}\cdot\nabla\Phi}{\dot{\chi}}=(\partial_\theta+\dot{q}\,v_0 t\,\partial_x)\,\Phi=f\exp\{i\alpha(x-\dot{q}\,v_0 t\,\theta)\}\cdot\sum_n\exp\{i\alpha\dot{q}\,v_0\,n\,N\,t\}\,F_\theta(\theta-nN)\sim 0(1)\,.$$

Thus, the test functions satisfy the conditions previously imposed.

We can write Φ in a different form

$$\Phi=N^{-1}f e^{i\alpha x}\sum_m\exp\{2\pi i\,m\,\theta/N\}\cdot\int_{-\infty}^{\infty}\exp\{-i(2\pi m/N+\alpha\dot{q}\,v_0 t)\,\eta\}\,F(\eta)\,\mathrm{d}\eta\,.\tag{4}$$

Then, if $A(\theta)$ is a periodic function of θ (period N), we can easily derive

$$A(\theta)\,\Phi(\theta) = N^{-1} f e^{i\alpha x} \sum_m \exp\{2\pi i\, m\,\theta/N\} \tag{5}$$
$$\cdot \int_{-\infty}^{\infty} \exp\{-i(2\pi m/N + \alpha \dot{q} v_0 t)\,\eta\}\, A(\eta)\, F(\eta)\, \mathrm{d}\eta .$$

Thus, taking into account the properties of f (localization and slow dependance on t), we obtain

$$\delta W_0 = 2\varepsilon^3 v_0^3 \alpha^2 \overline{|f|^2} \int_{-\infty}^{\infty} [B^{-2} \dot{\chi}^4 |\nabla\varphi - \dot{q}\,\eta\,\nabla v)|^2 |F_\eta|^2$$
$$- 2\dot{p}(\varkappa_v + \dot{q}\,\eta\,\varkappa_\varphi)\,|F|^2]\,\mathrm{d}\eta , \tag{6}$$

where

$$\overline{|f|^2} = \frac{\varepsilon^3}{4} \int_{-\varepsilon^{-1}}^{\varepsilon^{-1}} \mathrm{d}t \int_{-\varepsilon^{-2}}^{\varepsilon^{-2}} \mathrm{d}x\, |f|^2 .$$

Since F is arbitrary in $L_2(-\infty, \infty)$, we can now minimize δW_0 with respect to F and obtain (with a Lagrange multiplier λ) the Euler equation

$$\frac{\mathrm{d}}{\mathrm{d}\eta} \frac{\dot{\chi}^4}{B^2} |\nabla\varphi - \dot{q}\,\eta\,\nabla v|^2 F_\eta \tag{7}$$
$$+ 2\dot{p}\,(\varkappa_v + \dot{q}\,\eta\,\varkappa_\varphi)\,F + \lambda F = 0.$$

Thus

$$\delta W_0 = 2\varepsilon^3 v_0^3 \alpha^2 \lambda \int_{-\infty}^{\infty} |F|^2\,\mathrm{d}\eta .$$

Hence, we have instability if $\lambda_{\min} < 0$, where $\lambda_{\min}$ is the lowest eigenvalue of Equation (7). Equation (7) can be written in a different form

$$B \frac{\mathrm{d}}{\mathrm{d}l} \frac{B}{|\nabla v|^2} \left[1 + \left(\frac{|\nabla v|^2}{B} \int_{F_i}^{l} c \frac{\mathrm{d}l}{B}\right)^2\right] \tag{9}$$
$$+ 2\dot{p}\left(\frac{\varkappa^v}{|\nabla v|^2} - \frac{\varkappa_\varphi}{\dot{\chi}} \int_{l}^{} c \frac{\mathrm{d}l}{B}\right) F + \lambda F = 0 ,$$

where l is the length along the localization line and

$$c = |\nabla v|^{-4}\, \nabla v \times \boldsymbol{B} \cdot \nabla \times (\nabla v \times \boldsymbol{B}), \quad \varkappa^v = \varkappa \cdot \nabla v .$$

It is then easily seen that this equivalent to the equation derived by Connor et al. [3] for the case of axial symmetry and the conclusions which lead to the known Mercier's criterion in Ref. [3] are also valid here. However, Eq. (9) is valid not only for axisymmetric equilibria but for any three-dimensional equilibrium.

It is a pleasure to thank J. Nührenberg for several useful discussions and D. Lortz and G. O. Spies for interesting conversations.

This work was performed under the terms of the agreement on association between the Max-Planck-Institut für Plasmaphysik and EURATOM.

[1] C. Mercier, EUR-CEA-FC — 692 (1973).
[2] C. Mercier and H. Luc, in "Lectures in Plasma Physics" (Commission of the European Communities. Directorate General Scientific and Technical Information, Luxembourg, 1974).
[3] J. W. Connor, R. J. Hastie, and J. B. Taylor, Phys. Rev. Lett. **40**, 396 (1978).
[4] D. Dobrott, D. B. Nelson, J. M. Greene, A. H. Glasser, M. S. Chance, and E. A. Frieman, Phys. Rev. Lett. **39**, 943 (1977).
[5] B. Coppi, Phys. Rev. Lett. **39**, 939 (1977).
[6] J. B. Bernstein, E. A. Frieman, M. D. Kruskal, and R. M. Kulsrud, Proc. Roy. Soc., London, Ser. A **244**, 17 (1958).
[7] B. Hamada, Nucl. Fusion **2**, 23 (1962).
[8] D. Lortz, Nucl. Fusion **15**, 49 (1975).